

Occurrence of a quasicrystalline phase in the Ti-Fe(Ni)-Si system

P. Mandal, R. S. Tiwari, and O. N. Srivastava

Department of Physics, Banaras Hindu University, Varanasi-221 005, India

(Received 24 July 1992; revised manuscript received 17 November 1992)

Extensive studies have been carried out regarding the possible occurrence of the icosahedral phase in the rapidly solidified Ti-Fe(Ni)-Si alloy system in a wide range of compositions. Transmission electron microscopy and x-ray-diffraction data reveal the formation of the icosahedral phase in $\text{Ti}_{68}\text{Fe}_{26-x}\text{Ni}_x\text{Si}_6$ where $x \leq 9$. In addition to the sharp diffraction spots conforming to the icosahedral point group, subtle structural features manifested by spot shifts, asymmetry in the spot shape, and diffuse intensity have been observed in electron-diffraction patterns. A particular composition has been found, $\text{Ti}_{56}\text{Fe}_3\text{Ni}_{23}\text{Si}_{16}$, that exhibits a metastable fcc phase with lattice parameter close to 1.79 nm. We also report on structural transformations of the icosahedral and metastable crystalline phases originating as a result of annealing (icosahedral and metastable crystalline phases change to the equilibrium crystalline phase at 900°C).

I. INTRODUCTION

Ever since the discovery of the icosahedral quasicrystalline phase in a rapidly solidified Al-Mn alloy,¹ one of the main areas of study has been the exploration of systems exhibiting quasicrystalline (QC) and related phases. The number of alloy systems exhibiting such phases is quite large.²⁻⁶ Among these, the Ti-3d transition-metal-based (Fe, Ni, Co, etc.) alloy systems are rather interesting. Dong *et al.*⁷ reported the existence of a QC phase manifested by icosahedral symmetry in the Ti-Fe system. Similarly, Kelton, Gibbons, and Sabes⁸ reported the occurrence of an icosahedral phase in Ti-Co and related systems. However, the case of Ti-Ni (Ref. 9) remains rather subtle. Clear-cut and unambiguous evidence for the existence of a QC phase in this particular system has not been obtained so far. Kelton, Gibbons, and Sabes reported that the QC phase is absent in the Ti-Ni system.⁸ Later, Zhang, Ye, and Kuo found evidence of a QC phase in the vanadium-substituted versions of Ti-Ni, i.e., in $(\text{Ti}_{1-x}\text{V}_x)_2\text{Ni}$ alloys.¹⁰ Recently, some studies have been undertaken at specific compositions of Ti-Ni and Ti-Ni-Si (Ref. 11) as well as Ti-Fe-Ni-Si;^{12,13} systems possibly exhibiting an icosahedral phase.

We have made rather detailed investigations on Ti-Fe (Ref. 14) and related systems,^{15,16} and keeping in mind the above background for the Ti-Ni, Ti-Ni-Si, and Ti-Fe-Ni-Si systems at specific compositions with regard to the existence of the icosahedral quasicrystalline phase, we decided to undertake a detailed investigation of these employing both the x-ray-diffraction (XRD) and transmission-electron-microscopy (TEM) techniques.

The above-mentioned rapidly solidified alloys, with particular emphasis on the Ti-Fe-Ni-Si system, have been synthesized. A detailed structural characterization of all these specimens was carried out. To unravel the structural characteristics, including the existence of the icosahedral phase and possible metastable phases in these systems, several runs of the synthesis and structural characterization of the rapidly quenched alloys were made. In order to obtain unequivocal evidence for the oc-

currence of the quasicrystalline phase in these alloy systems, each of the alloy systems has been investigated under a wide range of composition and cooling rates. Based on the concept of the important physical parameter (e/a) the electron-atom ratio, which is known broadly to predict the specific compositions at which QC phases could exist¹⁷⁻²⁰ (in Al-transition-metal-based systems, e/a varies from 1.5 to 2.5), we have been able to achieve the specific composition at which the icosahedral phase becomes stabilized in the present systems. The determined compositions correspond to $\text{Ti}_{68}\text{Fe}_{26-x}\text{Ni}_x\text{Si}_6$, $x \leq 9$.

II. EXPERIMENTAL DETAILS

Starting from high-purity constituent elements of titanium, silicon (99.99%), iron (99.9%), and nickel (99.9%), bulk specimens of Ti-Ni, Ti-Ni-Si, and Ti-Fe-Ni-Si with various compositions have been synthesized by rf-induction melting in a previously outgassed graphite crucible under a controlled argon atmosphere. The master alloy ingots prepared in this way were melted again, and in the molten condition each of the alloy ingots was kept for a further period of heating which lasted at least 30 min to ensure homogenization. The homogenized ingots were subsequently crushed and placed in a quartz nozzle of ~ 1 cm internal diameter with a circular orifice of ~ 1 mm diameter and then melt spun onto a copper wheel (~ 14 cm diameter), rotating at a speed of about 20–30 m/sec, depending upon the system, to produce ribbons that were ~ 2 mm in width and about 40 μm in thickness. During melt spinning, the entire apparatus was enclosed in a steel enclosure through which argon flowed continuously at an over pressure of 50 atm so as to prevent oxidation of the ribbons after ejection from the nozzle. Ribbons of each of the specimens were subjected to x-ray-diffraction characterization employing a PW-1710 Philips x-ray diffractometer. The experimental conditions and parameters such as sample size, ratings of x-ray (30 kV, 20 mA) and other diffractometer parameters (scan speed, counting steps, etc.) were kept constant

for all the diffraction experiments performed on different samples. Specimens for transmission-electron microscopy were electrolytically thinned using an electrolyte of 10% HClO_4 in ethanol at -20°C and examined in a Philips CM-12 electron microscope. The elemental compositions of the specimens were checked by employing an electron microscope in the scanning TEM (STEM) mode employing a PV-9900 energy-dispersive x-ray analyzer.

III. RESULTS AND DISCUSSION

We have synthesized Ti-Ni, Ti-Ni-Si, and Ti(Si)-Fe(Ni), i.e., Ti-Fe-Ni-Si alloy systems under varying experimental conditions such as compositions and cooling rates. For each composition several runs on the synthesis of the master alloys as well as melt-spun alloys were made. Typical cooling rates employed corresponded to about 20–30 m/sec (see Table I). The gross structural characteristics of the Ti_2Ni , $\text{Ti}_2\text{Ni}(\text{Si})$, and $\text{Ti}_{56}\text{Fe}_5\text{Ni}_{23}\text{Si}_{16}$ alloys were carried out through the x-ray-diffraction technique. The representative XRD patterns are shown in Fig. 1. The analysis and indexing of the x-ray-diffraction pattern shown in Fig. 1(a) reveal that the structure of the rapidly solidified $\text{Ti}_{68}\text{Ni}_{26}\text{Si}_6$ alloy corresponds to a fcc structure with a lattice parameter $a = 1.13$ nm, which is close to the known equilibrium crystalline phase of Ti_2Ni . The XRD patterns shown in Figs. 1(b) and 1(c) are from a $\text{Ti}_{56}\text{Fe}_5\text{Ni}_{23}\text{Si}_{16}$ alloy with quenching rates of 20 and 45 m/sec, respectively. The diffractogram resulting from a

higher quenching rate (45 m/sec) of this alloy clearly shows the amorphous nature [Fig. 1(c)]. Figure 1(b) has been successfully indexed in terms of the fcc structure with $a \approx 1.79$ nm. Since for an unambiguous identification of the icosahedral phase electron-diffraction patterns manifesting undistorted representation of the reciprocal lattice are necessary, we proceeded to explore the alloys through transmission-electron-microscopic techniques, with particular emphasis on selected area and convergent-beam electron diffractions. Typical selected-area electron-diffraction (SAD) patterns corresponding to Ti_2Ni and $\text{Ti}_2\text{Ni}(\text{Si})$, shown in Fig. 2, have been found to be compatible with the observed XRD results. The SAD patterns corresponding to the rapidly solidified $\text{Ti}_{56}\text{Fe}_5\text{Ni}_{23}\text{Si}_{16}$ alloy are shown in Figs. 3(a)–3(c). These patterns, which are consistent with the XRD results, represent a fcc phase with $a \approx 1.79$ nm. The microstructure [see Fig. 3(c)] depicts the spherulitic morphology of the crystalline phase with grain size ~ 0.3 – 1.0 μm . The homogeneous nature of the phase may be inferred from microstructural observations. It is worthwhile mentioning that in the present case the existence of the fcc phase ($a \approx 1.79$ nm) has been established based on XRD as well as TEM results.

A systematic investigation was carried out of the quaternary Ti-Fe-Ni-Si system with a wide composition range to explore the occurrence of the icosahedral phase. Since the Hume-Rothery rules (Brillouin-zone-Fermi-surface interactions) are known to predict broadly^{17–20} the specific composition range at which the icosahedral phase may occur in several alloy systems, we derived the feasible compositions based on these rules. Thus these

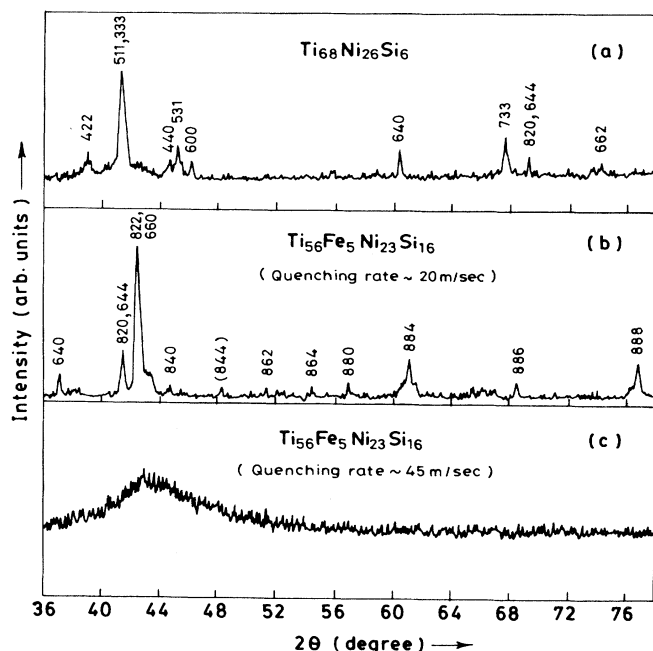


FIG. 1. X-ray-powder-diffraction patterns of the rapidly solidified alloys: (a) $\text{Ti}_{68}\text{Ni}_{26}\text{Si}_6$, (b) $\text{Ti}_{56}\text{Fe}_5\text{Ni}_{23}\text{Si}_{16}$ (medium quenching rate ~ 20 m/sec), and (c) $\text{Ti}_{56}\text{Fe}_5\text{Ni}_{23}\text{Si}_{16}$ (higher quenching rate ~ 45 m/sec). The analysis of the x-ray-diffraction patterns reveal fcc structures with $a \sim 1.13$ nm for $\text{Ti}_2\text{Ni}(\text{Si})$ and $a \approx 1.79$ nm for $\text{Ti}_{56}\text{Fe}_5\text{Ni}_{23}\text{Si}_{16}$. Indexing of the XRD peaks has been indicated.

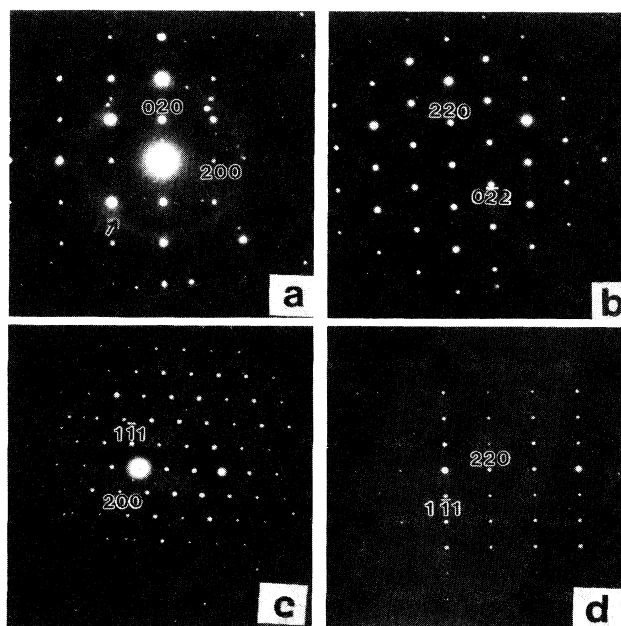


FIG. 2. Selected-area electron-diffraction patterns from the stable fcc ($a \sim 1.13$ nm) phase of $\text{Ti}_{68}\text{Ni}_{32}$ alloy with halos representing the (a) amorphousness and (b)–(d) $\text{Ti}_{68}\text{Ni}_{26}\text{Si}_6$ alloy.

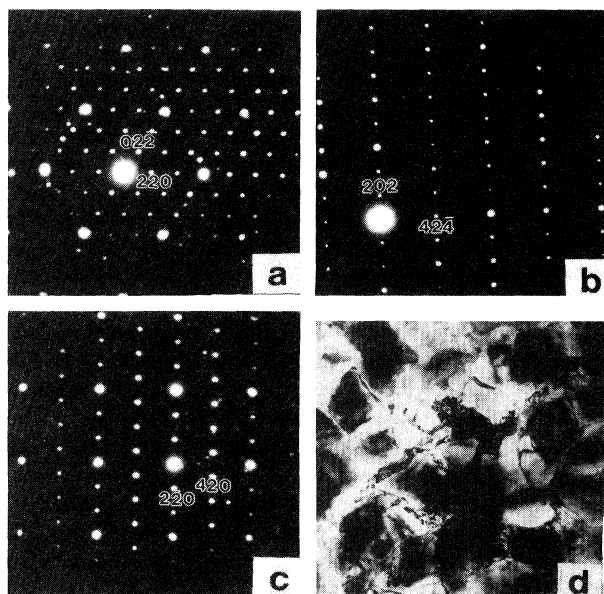


FIG. 3. Selected-area electron-diffraction patterns from a metastable crystalline (fcc with $a \approx 1.79$ nm) phase of $\text{Ti}_{56}\text{Fe}_5\text{Ni}_{23}\text{Si}_{16}$ showing (a) $[111]$, (b) $[141]$, and (c) $[001]$ sections of the corresponding reciprocal lattice. (d) TEM micrograph bringing out the crystalline morphology.

compositions were selected which gave electron-atom ratios (e/a) around 2.2 where the occurrence of the icosahedral phase were thought to be most likely.^{17–20}

Accordingly, bulk as well as melt-spun alloys of Ti(Si)-Fe(Ni) with the composition deduced based on the foregoing e/a considerations have been synthesized. We then proceeded to characterize the melt-spun quaternary Ti-Fe-Ni-Si system, employing both x-ray diffraction and transmission-electron microscopy (embodying imaging and diffraction modes). Detailed structural characterizations suggest the specific composition range for which the icosahedral phase occurs, and it corresponds to $\text{Ti}_{68}\text{Fe}_{26-x}\text{Ni}_x\text{Si}_6$, $x \leq 9$. These compositions were confirmed through elemental analysis employing the energy-dispersive x-ray analysis (EDAX) technique. A representative EDAX spectrum is shown in Fig. 4. The observed composition corresponds to $\text{Ti}_{68.5}\text{Fe}_{20}\text{Ni}_{5.5}\text{Si}_6$, within the limits of experimental error. A representative x-ray-diffraction pattern of these alloys is shown in Fig. 5. A rather remarkable result invariably obtained for Ti-Fe-Ni-Si with compositions corresponding to $\text{Ti}_{68}\text{Fe}_{26-x}\text{Ni}_x\text{Si}_6$, $x \leq 9$, was the occurrence of diffraction patterns with a fivefold (tenfold in diffraction patterns) symmetry characteristic of quasicrystalline phases. A representative selected-area electron-diffraction pattern is shown in Fig. 6(a). With the help of large-angle tilting experiments in the TEM, twofold and threefold symmetries shown in Figs. 6(b) and 6(c) were obtained employing selected-area electron diffraction. The analysis of the fivefold diffraction pattern coupled with twofold and

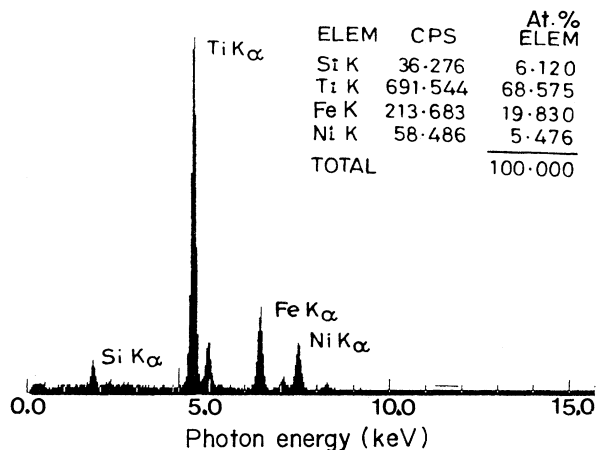


FIG. 4. Representative EDAX spectrum of the icosahedral phase bringing out the composition which is nearly stoichiometric.

threefold diffraction patterns clearly revealed the occurrence of the icosahedral phase in the $\text{Ti}_{68}\text{Fe}_{26-x}\text{Ni}_x\text{Si}_6$ ($x \leq 9$) alloys. The TEM imaging [Fig. 6(d)] also revealed an icosahedral-phase-type mottled microstructural feature.

After getting parameters for the icosahedral phase from TEM observations, the XRD patterns (Fig. 5) of $\text{Ti}_{68}\text{Fe}_{26-x}\text{Ni}_x\text{Si}_6$ ($x \leq 9$) were analyzed and was indexed based on a biphasic material with both the icosahedral phase and the stable crystalline (fcc) phase of (Fe,Ni) Ti_2 type ($a \sim 1.13$ nm) present. The peaks of the XRD pattern are labeled by the indices of the corresponding phases. The volume fraction and average grain size of the icosahedral phase in $\text{Ti}_{68}\text{Fe}_{26}\text{NiSi}_5$ was found to be about 90% and 0.5–2.0 μm , respectively. Whereas the volume fraction and average grain size of the icosahedral phase for the $\text{Ti}_{68}\text{Fe}_{18}\text{Ni}_9\text{Si}_5$ alloy (higher Ni concentra-

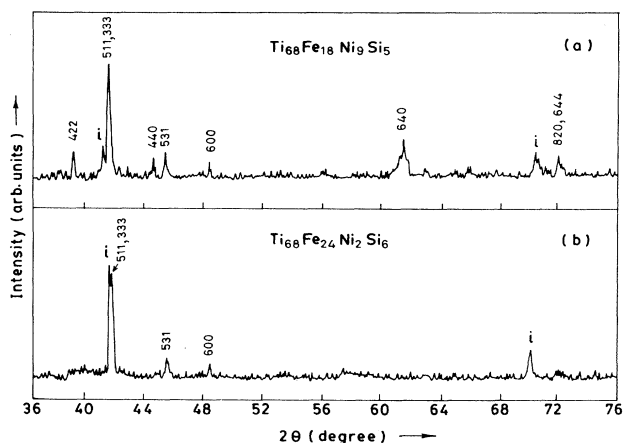


FIG. 5. Representative x-ray-powder-diffraction patterns of the as-quenched (a) $\text{Ti}_{68}\text{Fe}_{23}\text{Ni}_3\text{Si}_6$ and (b) $\text{Ti}_{68}\text{Fe}_{18}\text{Ni}_9\text{Si}_5$. Icosahedral peaks are labeled as i and the crystalline [fcc of (Fe,Ni) Ti_2 with $a = 1.13$ nm] peaks have also been outlined.

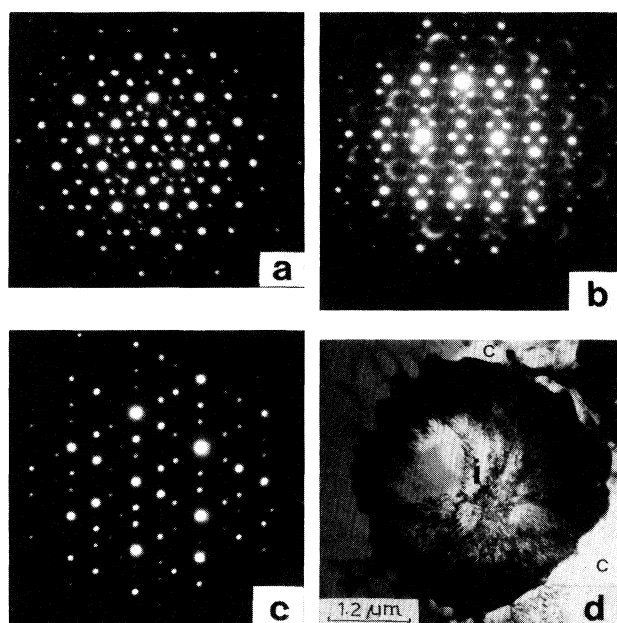


FIG. 6. Selected-area electron-diffraction patterns exhibiting the (a) fivefold, (b) twofold, and (c) threefold rotational symmetries characteristic of the icosahedral phase from the as-quenched Ti-Fe(Ni)-Si material. (d) A representative transmission electron micrograph of an as-spun $\text{Ti}_{68}\text{Fe}_{23}\text{Ni}_3\text{Si}_6$ alloy depicting the mottledlike morphology of the icosahedral grains labeled as *i* and featureless crystalline grains as *c*. Note the anisotropic nature (triangular shape) and distortion of diffraction spots [(a)]; arcs of diffuse intensity [(b)] in the diffraction patterns are also visible.

tion) was found to be $\sim 5\%$ and less than $0.5 \mu\text{m}$, respectively. For greater than 9 at. % Ni, the icosahedral phase was invariably absent. These observations clearly suggest that as the concentration of Ni in the Ti(Si)-Fe(Ni) system decreases, the volume fraction of the icosahedral phase increases.

A special feature of the observed icosahedral phase is that it always manifests itself in the form of a disordered phase. The evidence of disorder is manifested by the occurrence of either various subtle features such as spot anisotropy, shifting, and deviation from perfect icosahedral symmetry [see Fig. 6(a)] or diffuse intensity [see Fig. 6(b)] in diffraction patterns. Further evidence of disorder is shown in Figs. 7(a)–7(c), which bring out the icosahedral symmetry in mirror orientations. The asymmetries in the spot shape, shift of the spots, intensity distributions, and locations of the arcs have been found to be qualitatively similar to the earlier reported Ti-transition-metal-based alloy systems.^{15,16,21,22}

In order to check the thermal stability and the structural relationship of the phases, the as-quenched $\text{Ti}_{56}\text{Fe}_5\text{Ni}_{23}\text{Si}_{16}$ alloy, which exhibits a fcc phase with a lattice parameter close to 1.79 nm, and the icosahedral phase in $\text{Ti}_{68}\text{Fe}_{26-x}\text{Ni}_x\text{Si}_6$ ($x \leq 9$) were annealed isothermally at $900 \pm 10^\circ\text{C}$ for 30 min in an argon atmosphere. The x-ray-diffraction characterization of the an-

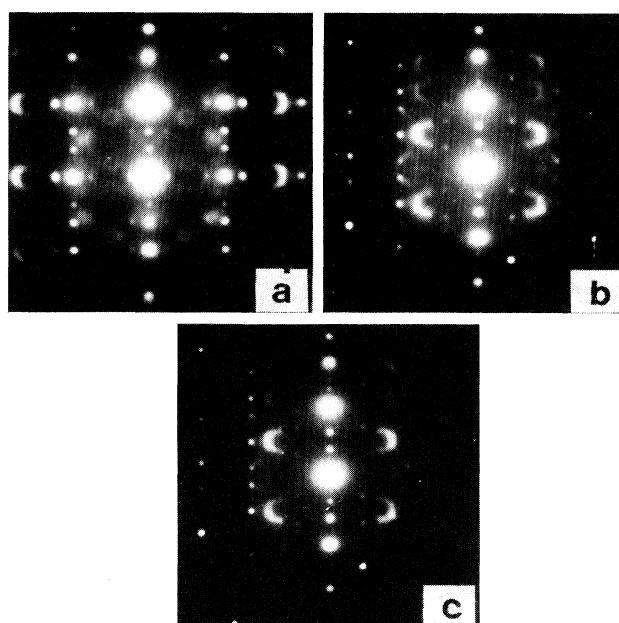


FIG. 7. (a)–(c) Representative SAD patterns from as-quenched $\text{Ti}_{68}\text{Fe}_{26-x}\text{Ni}_x\text{Si}_6$, $x \leq 9$, showing the mirror-symmetry orientations of the icosahedral phase. Note the arcs of diffuse scattering manifesting the disorder.

nealed ribbons has revealed the structural transformation of the icosahedral and metastable crystalline phases. It is interesting to note that both of these transform to the stable fcc phase with lattice parameter ~ 1.13 nm. This transformation reveals the metastable nature of the fcc phase ($a \approx 1.79$ nm) as well as that of the icosahedral phase.

Even though the icosahedral quasicrystalline phase may be present in rapidly solidified $\text{Ti}_{56}\text{Fe}_5\text{Ni}_{23}\text{Si}_{16}$ alloys as reported by earlier workers,^{11–13} our investigations based on x-ray diffraction and TEM seem to suggest that the dominant phase observed in this alloy corresponds to a metastable fcc phase with lattice parameter ≈ 1.79 nm. Following the Hume-Rothery rules (e/a ratios), we have deduced the specific compositions at which icosahedral phase is most likely to occur. For the range of e/a values 2.10–2.40, the occurrence of the icosahedral phase has actually been found. A list of Ti-Ni, Ti-Ni-Si, and Ti-Fe-Ni-Si alloy systems with specific compositions along with the corresponding average electron-per-atom concentration are given in Table I. Since in the present alloy systems transition metals are involved, a charge transfer to their d bands is allowed for the compensation of the unpaired spins of d electrons. We have, therefore, used elemental valencies (see Table II) assigned by Raynor.²³ It may be pointed out that the range of determined e/a values is close to those where the icosahedral phase has been found to occur by earlier workers.^{17–20,24} It should be noted that the e/a values for Ti_2Ni , $\text{Ti}_2\text{Ni}(\text{Si})$, and $\text{Ti}_{56}\text{Fe}_5\text{Ni}_{23}\text{Si}_{16}$ are 2.52, 2.80, and 2.61, respectively. All these differ from the predicted range of 2.1–2.4, where the icosahedral phase has been suggested to occur. Thus the dominant occurrence of the crystalline (fcc) phases in

TABLE I. List of alloy systems (binary, ternary, quaternary) along with chemical composition, e/a values, and some other experimental parameters.

Alloy system	Chemical composition (through EDAX)	e/a	Quenching rate (m/sec)	Phases obtained	Remarks
Ti-Ni	Ti ₆₈ Ni ₃₂	2.52	25	Stable fcc phase of Ti ₂ Ni ($a \sim 1.127$ nm) and amorphous phase	Grain size $\sim 0.3 \mu\text{m}$
Ti-Ni-Si	Ti ₆₈ Ni ₂₆ Si ₆	2.80	28	Stable fcc phase of Ti ₂ Ni ($a = 1.13$ nm)	Average grain size $0.5\text{--}1.5 \mu\text{m}$ and mottledlike morphology of the grains
Ti-Fe-Ni-Si	Ti ₅₆ Fe ₅ Ni ₂₃ Si ₁₆	2.61	20	Dominantly metastable fcc phase with $a \approx 1.79$ nm	Average grain size $\sim 0.3\text{--}1.0 \mu\text{m}$
			45	Microcrystalline and amorphous phases	Grain size $\sim 0.1 \mu\text{m}$
Ti-Fe(Ni)-Si	Ti ₆₈ Fe ₅ Ni ₂₁ Si ₁₆	2.70	28	Stable fcc (~ 1.13 nm) and metastable fcc phases ($a \approx 1.79$ nm)	Volume fraction of stable fcc $\sim 20\%$
	Ti ₆₈ Fe ₁₈ Ni ₉ Si ₅	2.39	28	Stable fcc phase of Ti ₂ (Ni/Fe) and icosahedral phase	Maximum grain size of icosahedral phase $\sim 0.5 \mu\text{m}$, volume fraction of icosahedral phase, $\sim 5\%$
	Ti ₆₈ Fe ₂₁ Ni ₅ Si ₆	2.37	30	Icosahedral and stable fcc phases of Ti ₂ (Fe/Ni)	Volume fraction of icosahedral phases, $\sim 70\%$
	Ti ₆₉ Fe ₂₂ Ni ₄ Si ₅	2.35	28	Icosahedral and stable fcc phases of Ti ₂ (Fe/Ni)	Volume fraction of icosahedral phase, $\sim 75\%$
	Ti ₆₇ Fe ₂₆ Ni ₂ Si ₅	2.18	32	Icosahedral and stable fcc phases of Ti ₂ (Fe/Ni)	Volume fraction of icosahedral phase, $\sim 80\%$
	Ti ₆₈ Fe ₂₆ NiSi ₅	2.22	28	Icosahedral and approximant phases of higher order	Volume fraction of icosahedral phase, $\sim 90\%$, average grain size $\sim 0.5\text{--}1.5 \mu\text{m}$

the Ti-Ni and related systems is explicable based on the e/a criterion. The present results thus reveal that the Ti-Fe(Ni)-Si alloy system with specific composition Ti₆₈Fe_{26-x}Ni_xSi₆, $x \leq 9$, where the icosahedral phase occurs, can be taken as electron phase.

IV. CONCLUSIONS

In the present investigation, a systematic study of the Ti-Fe-Ni-Si and other related systems with regard to the occurrence of the icosahedral and metastable phases has been carried out employing both XRD and TEM techniques. The salient results obtained from the present studies relate to the occurrence of the icosahedral quasi-crystalline phase in the Ti-Fe-Ni-Si system for the composition Ti₆₈Fe_{26-x}Ni_xSi₆, with $x \leq 9$. This specific composition range has been deduced based on the Hume-Rothery e/a (Brillouin-zone-Fermi-surface interaction) criterion. Yet another result in the Ti-Fe-Ni-Si system in the specific composition Ti₅₆Fe₅Ni₂₃Si₁₆ corresponds to the dominant occurrence of a metastable fcc phase with a

lattice parameter close to 1.79 nm. As in other Ti-transition-metal-based alloy systems, silicon is important for the formation and stabilization of the icosahedral phase in the Ti-Fe(Ni) system. The observed icosahedral phase in the Ti-Fe(Ni)-Si system was found to be disordered. Phase transformations through annealing reveal that both the icosahedral and the metastable fcc ($a \approx 1.79$ nm) phases transform to the stable fcc ($a \sim 1.13$ nm) phase.

TABLE II. Elemental valencies [assigned by Raynor (Ref. 23)] adopted in the e/a calculation are listed. The negative valency of the transition metals signifies the charge transfer to their d bands for the compensation of the unpaired spins of d electrons.

Element	Valency
Ti	+4
Fe	-2.66
Ni	-0.61
Si	+4

ACKNOWLEDGMENTS

The authors would like to thank Professor A. L. Mackay for initial encouragement. Helpful discussions with Professor H. Wondratschek, Professor S. Lele, Dr.

G. V. S. Sastry, Dr. V. Srinivas, Dr. R. K. Mandal, and N. P. Lalla are gratefully acknowledged. We would like to express our gratitude to Professor A. R. Verma, Professor C. S. Jha, and Professor S. Ranganathan for encouragement. One of the authors (P.M.) gratefully acknowledges CSIR (New Delhi) for financial support.

-
- ¹D. Shechtman, I. Blech, D. Gratious, and J. W. Cahn, *Phys. Rev. Lett.* **53**, 1951 (1984).
²P. Ramachandrarao and G. V. S. Sastry, *Pramana* **25**, L225 (1985).
³L. Bendersky, *Phys. Rev. Lett.* **55**, 1461 (1985).
⁴K. Chattopadhyay, S. Ranganathan, N. Subbanna, and N. Thangaraj, *Scr. Metall.* **19**, 767 (1985).
⁵C. H. Chen and H. S. Chen, *Phys. Rev. B* **33**, 2814 (1986).
⁶A. P. Tsai, A. Inoue, and T. Masumoto, *J. Mater. Sci. Lett.* **7**, 322 (1988).
⁷C. Dong, Z. K. Hei, L. B. Wang, Q. H. Song, Y. K. Wu, and K. H. Kuo, *Scr. Metall.* **20**, 1155 (1986).
⁸K. F. Kelton, P. C. Gibbons, and P. N. Sabes, *Phys. Rev. B* **38**, 7810 (1988).
⁹Z. M. Stadnik, G. Stroink, K. Dini, and R. A. Dunlap, *J. Phys. F* **17**, 1403 (1987).
¹⁰Z. Zhang, H. Q. Ye, and K. H. Kuo, *Philos. Mag. A* **52**, L49 (1985).
¹¹R. Chatterjee and R. C. O'Handley, *Phys. Rev. B* **39**, 8128 (1988).
¹²R. A. Dunlap, R. C. O'Handley, M. E. McHenry, and R. Chatterjee, *Phys. Rev. B* **37**, 8484 (1988).
¹³D. Bahadur, V. Srinivas, R. A. Dunlap, R. C. O'Handley, and M. E. McHenry, *Philos. Mag. B* **60**, 871 (1989).
¹⁴P. Mandal, A. K. Singh, and O. N. Srivastava, *Cryst. Res. Technol.* **23**, K139 (1988).
¹⁵P. Mandal, R. S. Tiwari, and O. N. Srivastava, *Phys. Rev. B* **44**, 11 683 (1991).
¹⁶P. Mandal, R. S. Tiwari, and O. N. Srivastava *Philos. Mag. A* **63**, 617 (1991).
¹⁷P. A. Bancel and P. A. Heiney, *Phys. Rev. B* **33**, 1917 (1986).
¹⁸P. Villars, J. C. Phillips, and H. S. Chen, *Phys. Rev. Lett.* **57**, 3085 (1986).
¹⁹J. Friedel and F. Denoyer, *C. R. Acad. Sci. (Paris)* **305**, 171 (1987).
²⁰P. M. Ossi and D. C. Kothary, *J. Less-Common Met.* **171**, 221 (1991).
²¹P. C. Gibbons, K. F. Kelton, L. E. Levine, and R. B. Phillips, *Philos. Mag. B* **59**, 593 (1989).
²²X. Zhang and K. F. Kelton, *Philos. Mag. Lett.* **62**, 265 (1990).
²³G. V. Raynor, in *Progress in Metal Physics*, edited by Bruce Chalmers (Butterworths, London, 1949), Vol. 1, pp. 1–16.
²⁴P. Mandal, R. K. Mandal, R. S. Tiwari, and O. N. Srivastava, *Phys. Rev. B* **45**, 7521 (1992).

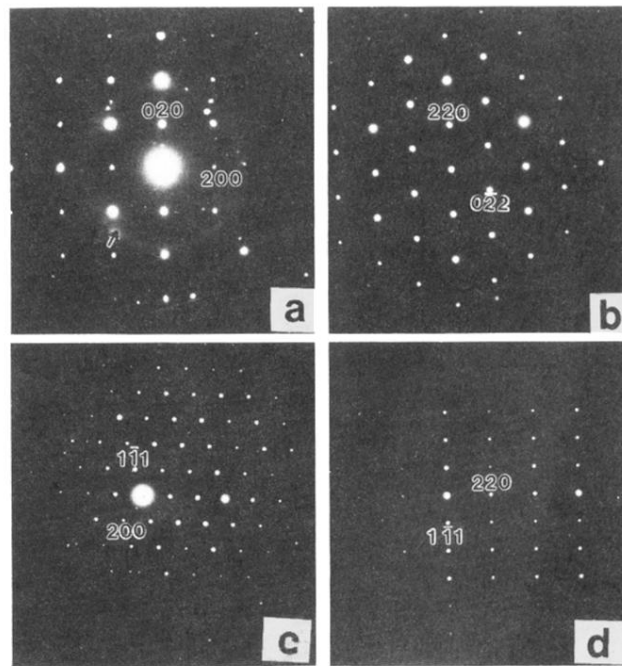


FIG. 2. Selected-area electron-diffraction patterns from the stable fcc ($a \sim 1.13$ nm) phase of $\text{Ti}_{68}\text{Ni}_{32}$ alloy with halos representing the (a) amorphousity and (b)–(d) $\text{Ti}_{68}\text{Ni}_{26}\text{Si}_6$ alloy.

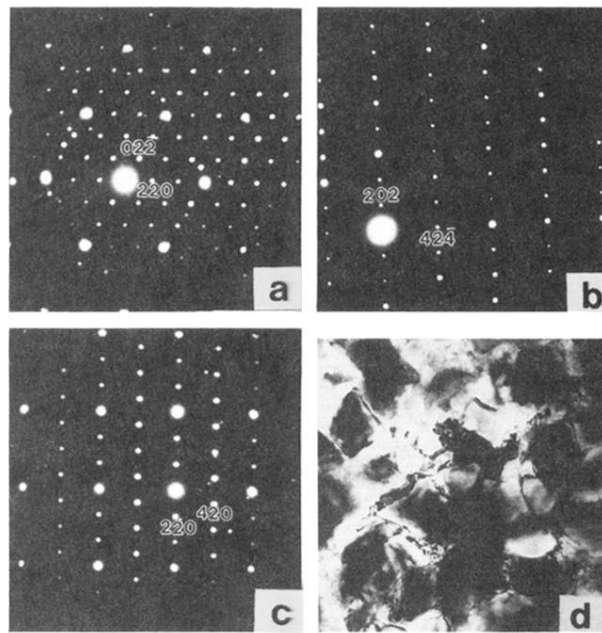


FIG. 3. Selected-area electron-diffraction patterns from a metastable crystalline (fcc with $a \approx 1.79$ nm) phase of $\text{Ti}_{56}\text{Fe}_5\text{Ni}_{23}\text{Si}_{16}$ showing (a) $[\bar{1}11]$, (b) $[1\bar{4}1]$, and (c) $[001]$ sections of the corresponding reciprocal lattice. (d) TEM micrograph bringing out the crystalline morphology.

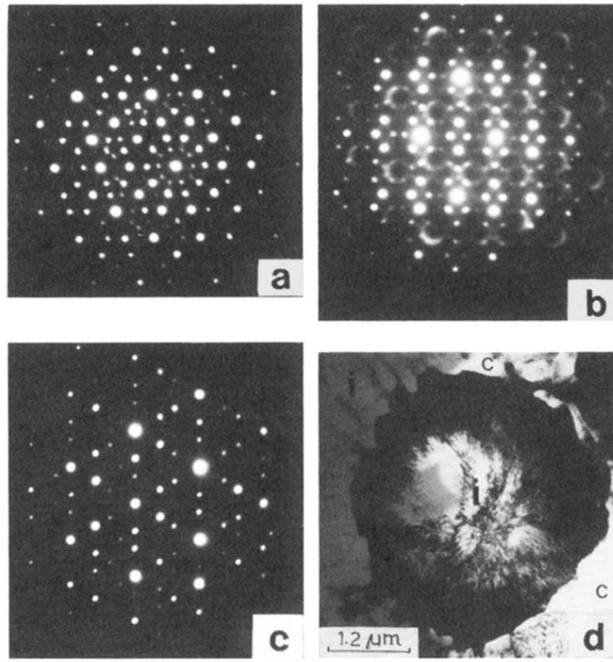


FIG. 6. Selected-area electron-diffraction patterns exhibiting the (a) fivefold, (b) twofold, and (c) threefold rotational symmetries characteristics of the icosahedral phase from the as-quenched Ti-Fe(Ni)-Si material. (d) A representative transmission electron micrograph of an as-spun $\text{Ti}_{68}\text{Fe}_{23}\text{Ni}_3\text{Si}_6$ alloy depicting the mottledlike morphology of the icosahedral grains labeled as *i* and featureless crystalline grains as *c*. Note the anisotropic nature (triangular shape) and distortion of diffraction spots [(a)]; arcs of diffuse intensity [(b)] in the diffraction patterns are also visible.

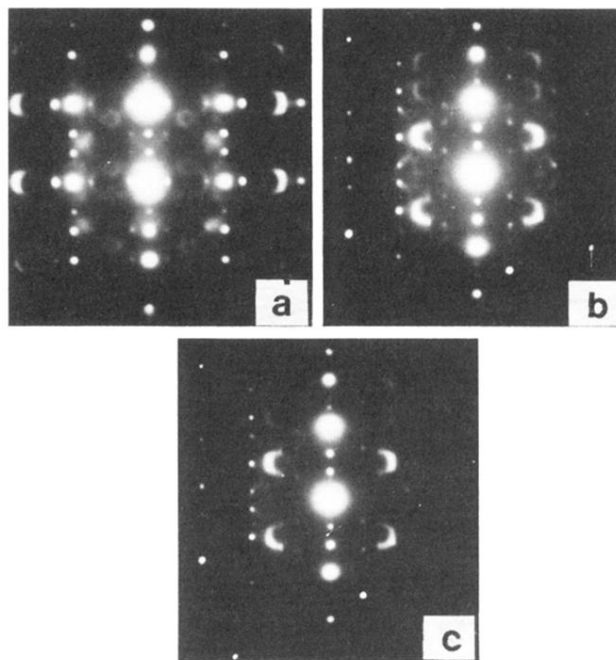


FIG. 7. (a)–(c) Representative SAD patterns from as-quenched $\text{Ti}_{68}\text{Fe}_{26-x}\text{Ni}_x\text{Si}_6$, $x \leq 9$, showing the mirror-symmetry orientations of the icosahedral phase. Note the arcs of diffuse scattering manifesting the disorder.